



# Design method for masonry structures retrofitted with steel reinforced plaster

Manuela Scamardo<sup>a,\*</sup>, Sara Cattaneo<sup>a,b</sup>, Pietro Crespi<sup>a</sup>, Luigi Biolzi<sup>a</sup>

<sup>a</sup> Department of Architecture, Built Environment and Construction Engineering, Politecnico di Milano, 20133, Milan, Italy

<sup>b</sup> Construction Technologies Institute, Italian National Research Council (ITC-CNR), 20098, San Giuliano Milanese, Italy

## ARTICLE INFO

### Keywords:

Masonry  
Overlay retrofitting system  
Steel reinforced plaster  
Diagonal compression test  
Analytical model

## ABSTRACT

In this paper an analytical approach for the design and assessment of masonry structures retrofitted with steel reinforced plaster (SRP) is proposed. The aim of the proposed method is to consider the main parameters affecting the performance of the strengthened wall (such as masonry properties, plaster properties, spacing and number of connectors) and provide a general formulation for practitioners to use in the design of SRP retrofitting interventions in place of the common empirically-based numerical coefficients proposed by the Italian Standard. The approach is developed starting from the experimental results of diagonal compression tests performed on clay brick walls retrofitted with SRP presented by the authors in previous studies. The maximum load is analytically predicted considering that the plaster and masonry layers work in parallel. A validation is conducted using additional experimental data available in literature. The obtained formulation is able to approximate the experimental values, being on the safe side against them in most of the cases. It is important to note that the method has been developed and validated using a limited number of experimental results. For this reason, adjustments may be needed for different types of masonry, plaster or anchor configurations.

## 1. Introduction

Seismic events in Italy [1–3] and worldwide [4–6] have revealed the high vulnerability of unreinforced masonry (URM) buildings with respect to the horizontal actions from tremors. Moreover, weathering, degradation phenomena, and differential settlement can lead to the necessity of improving the structural response of masonry walls to prevent damages and failures.

As a consequence, structural protection and rehabilitation of existing masonry buildings have gained more and more attention from the scientific community.

The efforts of researchers have been focused on two main topics: on one side, the structural analysis [7–10], which represents the best way to understand the building behavior, determine the structural safety, and identify the necessary remedial measures; on the other hand, the study and characterization of traditional or innovative retrofitting techniques to improve the seismic resistance [11–16]. The choice of the most appropriate retrofitting method should be made considering several aspects such as the (i) type of masonry base material, (ii) level of improvement needed, (iii) material compatibility; (iv) reversibility of the solution (especially in case of heritage-sensitive constructions); (v) cost. In the everyday practice, the latter represents one of the main leading guiding criteria and often it amounts much higher more than a choice for innovative materials and techniques compared to more traditional methods.

\* Corresponding author.

E-mail addresses: [manuela.scamardo@polimi.it](mailto:manuela.scamardo@polimi.it) (M. Scamardo), [sara.cattaneo@polimi.it](mailto:sara.cattaneo@polimi.it) (S. Cattaneo), [pietro.crespi@polimi.it](mailto:pietro.crespi@polimi.it) (P. Crespi), [luigi.biolzi@polimi.it](mailto:luigi.biolzi@polimi.it) (L. Biolzi).

State-of-the-art reviews on the existing retrofitting techniques of existing masonry structures are described in Refs. [11,12].

Among the common strengthening solutions, the application of a reinforced overlay [17–19] on the masonry surface is one of the most effective methods to provide enhancements in strength, stiffness, and deformation capacity, both in-plane and out-of-plane. It consists in confining the exterior sides of the masonry construction with reinforcement grids (e.g. steel or polymer) and a coating layer of plaster or adhesive. This method has the advantage of being easily applied to the wall, with limited costs if the more traditional configuration, i.e. with steel as reinforcement, is considered. The main drawback, however, is that the overlay brings a potentially significant increase of the structural mass, which represents a disadvantage in seismic prone areas. Moreover, its application is often not allowed in structures with architectural and historical value because it can harm the aesthetic appearance of the building.

Overlays can incorporate different types of reinforcement to increase their tensile strength and ductility [20]; steel reinforcement is the more conventional, while grids/mesh fabric from advanced fibers (e.g. carbon, glass, basalt) have been introduced more recently. When steel meshes are adopted, overlays are typically referred to as steel reinforced plasters (SRPs). In this case, the overlay (plaster) is made of cementitious mortars or concrete with 30–70 mm thickness. To transfer the shear stresses across the plaster-masonry interfaces and avoid buckling phenomena, steel connectors are fixed into pre-drilled holes to the masonry and connected to the steel mesh. Thereby, for the connectors, an anchor system suitable for use under seismic conditions should be used [21]. The reinforcement made with fiber reinforced polymers (FRP) shows a high strength-weight ratio and durability [22,23]. It may be used with organic or inorganic matrix material. Organic binders have the advantage of providing good adhesion between the composite and the masonry substrate, but compatibility issues and moisture movement inside the structural members can develop. Inorganic matrix composites [24–26] are instead gaining popularity for application on masonry due to their compatibility with the substrate and the limited thickness of the mortar layer required (about 10 mm). As an alternative to the introduction of the reinforcement meshes or grids, cementitious composites strengthened with synthetic or steel fibers may be adopted [27,28].

Despite the availability of innovative materials, traditional SRP remain one of the most largely employed conventional methods in everyday practice to strengthen common masonry constructions [29] because of its simple technology, the use of ordinary and inexpensive materials, and its effectiveness. The use of SRP has been introduced in Italy after the 1976 Friuli and 1980 Irpinia earthquakes, when it was suggested by a Standard [30] as a method to repair damaged masonry structures. The technique is currently listed by the Italian regulation [31,32] among the most common and effective retrofitting interventions for masonry buildings. Outside of Italy, references on the use of SRP for masonry retrofitting can be found, e.g. in the Greek Standards [33] or American Standards [34]. However, even if several technical codes recommend it as an effective retrofitting solution, it is difficult to find a proper mechanical characterization of the method in the scientific literature. Few studies have been published with limited experimental data [35–38]. Theoretical models able to establish the in-plane capacity of masonry walls strengthened with SRP have not been proposed for practical design, unlike other non-traditional retrofitting techniques as GFRP meshes [39] or steel fiber reinforced mortar coating [40], where analytical models have been presented. Moreover, existing codes do not cover the design with a systematic approach, sometimes providing only simple empirically-based numerical coefficients to account for SRP beneficial effects. This is also the case for the current Italian design guideline NTC 2018 [31,32], which recommends to adopt an amplification coefficient (suggested by the code according to the typology of studied masonry) to increase the resistance parameters and the elastic modulus. As an alternative, it suggests performing a more accurate evaluation of the SRP effect, accounting for the thickness and the mechanical properties of both masonry and plaster cover, without providing the required tools to the designer. The lack of accurate analytical and experimental information did not stop engineers and practitioners from using SRP in daily practice, with the consequence of often obtaining unconservative or uneconomical solutions for which the degree of safety is not known.

To resolve this issue, in this paper, an analytical model, based on mechanics of materials concepts, is proposed to predict the strength of retrofitted masonry walls. The method is for the design and assessment of SRP-strengthened masonry structures, focused on the evaluation of the wall's carrying capacity in terms of mechanical properties of the retrofitted masonry. The aim is to define a general formulation, which considers the main parameters that affect the performance of the strengthened wall, to be used by practitioners in the design of SRP retrofitting interventions. The method was developed starting from the experimental evidence presented by the authors in Refs. [37,41]. A total of ten unreinforced and retrofitted masonry clay brick walls were subjected to cyclic diagonal compression loading under displacement control, following established procedures [42–44]. Different thicknesses of walls (2 and 3 wythes) and plasters (30 and 50 mm) were tested. Reinforced plaster was applied symmetrically on both sides of the wall. The mechanical properties of the masonry and plaster, the configuration of the steel reinforcement, and the number of connectors were the same in all the tests. In addition, given the limited number of tested specimens, results from other authors of experiments performed on masonry walls retrofitted with SRP were used to evaluate the methodology [38,39].

## 2. Analytical method

The proposed method analytically predicts the maximum load of a diagonal compression test performed on a wall specimen strengthened with SRP. From the comparison between this value and the capacity of the unreinforced wall, it is possible to determine an amplification coefficient. In design, this factor is applied to the mechanical properties of the unstrengthened masonry in order to obtain the properties of the reinforced one.

The formulation was developed on the basis of the outcomes obtained in the experimental program presented in Refs. [37,41]. Two different phases were observed during the tests: (a) a first phase in which the composite section behaved as a monolithic one, with a perfect bond between the masonry and the plaster layer; in this stage, the compatibility in terms of deformations between the two materials was guaranteed by both the friction at the interface and the presence of the connectors; (b) a second phase in which the delamination of the plaster from the substrate took place, with the connectors playing a key role to avoid instability phenomena of the

plaster layer and reduce the out-of-plane displacements.

The experimental outcomes were used to develop, calibrate and validate the model. The final aim was to provide a simple and easy formulation for every-day practice to evaluate the capacity of SRP retrofitted walls.

Many parameters may affect the behavior of the reinforced specimen under diagonal compression test such as the thickness and the mechanical properties of the plaster layers, the configuration of the reinforcement (i.e., diameter and spacing of the steel net), and the number of connectors, making the prediction of the structural response a highly complex task. For this reason, some simplifying assumptions were considered.

The first hypothesis is that the wall is modeled as an equivalent diagonal strut. The equivalent strut model was developed and adopted by several authors (see e.g., Refs. [45,46]) to describe, in a simple way, the behavior of infill masonry panels subjected to horizontal loads. The experimental evidence proved that a frame, subjected to horizontal loads, tends to detach from the masonry infill in the region of two opposite diagonal corners. The other two corners remain instead in contact with the frame, so that, the masonry infill is subjected to diagonal compression and its structural behavior may be represented as a diagonal strut. The authors extended the same concept to the masonry panels subject to diagonal compression test, in which the opposite corners along the compressed diagonal are constrained by the loading system, and the other two are free to deform. The main difficulty of the method is to identify the equivalent strut in terms of geometrical dimension and, consequently, stiffness and strength. There are several approaches in the scientific literature to define the width  $w$  of the equivalent strut, from simple formulas which depends only on the diagonal length [47], to more complex analytical expressions, which involves several geometrical and mechanical parameters [48,49]. A review on the state-of-the-art of the topic may be found in Ref. [50]. The present approach follows the recommendation proposed by Stafford Smith [47], which suggested, on the basis of experimental data, that  $w$  should range between 0.10 and 0.25 of the strut length. In particular, the width of the strut was defined as:

$$w = 0.15L_d \quad (1)$$

with  $L_d$  length of the compressed diagonal (Fig. 1). The chosen value was validated using experimental results of diagonal compression tests performed on unreinforced masonry specimens. Other analytical models were excluded due to the necessity to introduce further parameters related to the r.c. frame (e.g., the contact length between panel and frame or the relative stiffness between the infill and the columns), which were not applicable.

The presence of the steel reinforcement is neglected. This assumption leads to a conservative evaluation of the wall response according to the results obtained in Ref. [51], in which it is proved that the steel mesh has a positive effect on the bearing capacity of the retrofitted wall.

One last assumption is made on the sectional behavior. The cross-section of the strut, in the case of the reinforced specimen, is a composite section (plaster – masonry – plaster). It is assumed that the different materials work in parallel and that the displacement compatibility at the interface between masonry and plaster is guaranteed thanks to the presence of the connectors. In terms of constitutive law, an elastic-plastic behavior for the plaster and an elastic-brittle behavior for the masonry are assumed. Fig. 2a and b represent the constitutive relations in terms of displacement (i.e. shortening or elongation) and axial force  $N$ . The compatibility between masonry and plaster layers is assumed (i.e.,  $\delta_m = \delta_p$ , where  $\delta_m$  and  $\delta_p$  are the generic displacements, i.e. shortening or elongation of the strut, of masonry and plaster, respectively). The ultimate displacement for masonry is named  $\delta_{m,u}$ , the displacement at the plaster yielding is called  $\delta_{p,y}$ . Considering that usually  $\delta_{m,u} > \delta_{p,y}$ , the maximum load of the composite section  $N_{max}$  associated to the diagonal compression test (Fig. 2c) may be evaluated as:

$$N_{max} = N_p + N_m \quad (2)$$

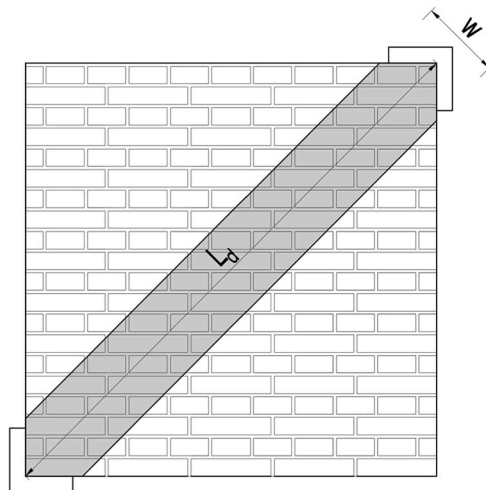


Fig. 1. Masonry as equivalent diagonal strut.

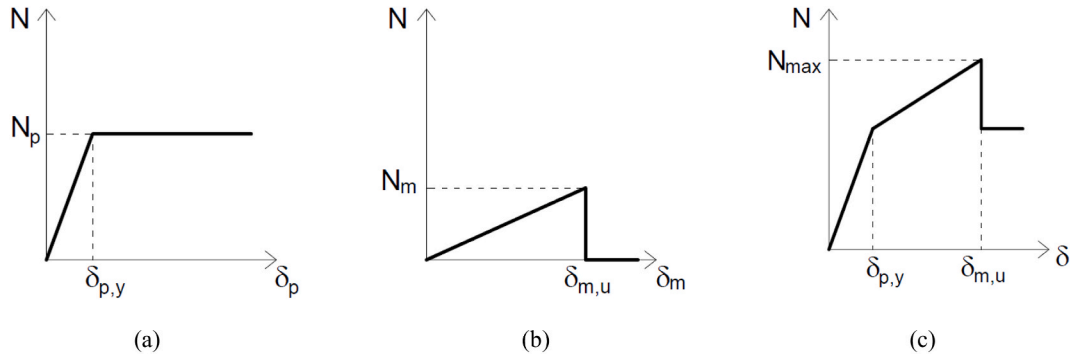


Fig. 2. Constitutive assumptions for (a) plaster, (b) masonry and (c) composite section.

where  $N_m$  and  $N_p$  are the maximum axial load in masonry and plaster, respectively.

The masonry strut maximum load  $N_m$  can be evaluated, using a simplified approach, as:

$$N_m = f_m \cdot w \cdot t_m \quad (3)$$

where  $f_m$  is the masonry compressive strength,  $w$  is the width of the strut and  $t_m$  is the masonry thickness.

According to the experimental evidence, in the evaluation of the plaster contribution under compression, two different failure modes must be considered: i) the failure for crushing, with maximum load  $N_{p,c}$ ; ii) the failure for buckling, which may happen after the detachment of the plaster at the masonry-plaster interface due to the high slenderness of the plaster layer, with maximum load  $N_{p,i}$ . Considering the two different plaster failure modes, the ultimate load for the retrofitted masonry  $N_{max}$  associated to the diagonal compression test will be:

$$N_{max} = \min\{2N_{p,i} + N_m, 2N_{p,c} + N_m\} \quad (4)$$

According to the approach suggested by the Italian Standard [31,32], the mechanical properties of the reinforced wall are evaluated by applying an increasing factor to the properties of the unreinforced masonry. The increasing factor  $\lambda$  is calculated as the ratio between the compression limit load  $N_m$  associated to the unreinforced masonry and the load  $N_{max}$ , which accounts for both masonry and plaster:

$$\lambda = \frac{N_{max}}{N_m} \quad (5)$$

As example, the shear strength  $\tau_{0,r}$  of the strengthened masonry will be evaluated as  $\tau_{0,r} = \lambda \cdot \tau_0$  with  $\tau_0$  shear strength of the unreinforced masonry wall.

The maximum loads associated to the different plaster failure modes are evaluated in the following section.

### 2.1. Plaster contribution

The limit load  $N_{p,c}$  associated with the crushing of the plaster is calculated as:

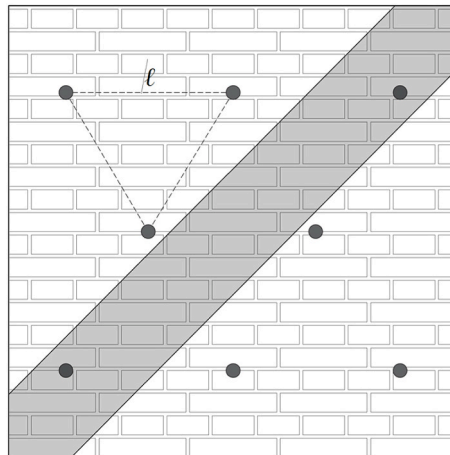


Fig. 3. Quincunx connector arrangement.

$$N_{p,c} = f_{c,r} \cdot w \cdot t_p \quad (6)$$

where  $t_p$  is the plaster layer thickness and  $f_{c,r}$  is its compressive strength, evaluated as:

$$f_{c,r} = v \cdot f_{ck} \quad (7)$$

where  $v$  is a strength reduction factor, defined according to Eurocode 2 §6.2.2 [52], which takes into account the effect of shear cracks on the compressive resistance  $f_c$ , and it is equal to:

$$v = 0.6 \left( 1 - \frac{f_{ck}}{250} \right) \quad (8)$$

with  $f_{ck}$  characteristic compressive cylinder strength of the plaster expressed in MPa.

In the evaluation of the instability phenomenon, the presence of connectors and initial imperfections must be taken into account since they may have a significant effect on the ultimate load.

The connectors play a fundamental role in the out-of-plane response of the plaster layer, by reducing the effective length of the diagonal strut. The most common connector configuration is represented in Fig. 3 where a quincunx disposition is adopted using equilateral triangle.

From a theoretical point of view, an analogy can be made between the diagonal strut representing the plaster layer constrained by the connectors and a longitudinal steel bar of a reinforced concrete column constrained by the hoops and subjected to axial force. For this reason, the analytical buckling model proposed by Papia and Russo [53,54] for the longitudinal reinforcement in reinforced concrete columns was adapted and used to evaluate the effect of the anchors on the critical load. The connectors were considered as unilateral elastic supports, whose stiffness was evaluated by adopting simple analytical formulas, which accounted for the geometrical and mechanical characteristics of the connector. The method proposed by Papia et al. [53] uses a discrete number of unilateral supports equally distributed along the bar (Fig. 4a), number that, in the case of SRP, is difficult to be determined since the anchors are not localized along the diagonal but spread over the specimen surface (Fig. 3). Moreover, according to the method, the critical load can only be determined using a numerical procedure, which results to be hard to apply in a retrofitting design process. The approach proposed by Russo [54] develops from the Papia buckling model, but adopts as constraint an equivalent elastic medium (Fig. 4b), similar to the Winkler soil, spreading the stiffness of discrete springs along the whole bar length, with the advantage that the critical load can be evaluated without a numerical procedure. Russo proved that the results were in good agreement with the one obtained with discrete constraints.

The use of a spread stiffness and the fact that no numerical procedure is required to find the critical load are great advantages considering the final goal of this research (i.e., providing an analytical approach to be used in the daily practice). According to the Russo formulation, the non-dimensional critical load  $c_{cr}$  can be evaluated as:

$$c_{cr} = \frac{2}{\pi^2} \sqrt{3\gamma} \quad (9)$$

where  $\gamma$  is defined as:

$$\gamma = \frac{\beta \ell^4}{E_{p,r} I_p} \quad (10)$$

with  $\beta$  stiffness of the equivalent elastic medium expressed as:

$$\beta = \frac{\alpha}{\ell} \quad (11)$$

with  $\ell$  distance between the connectors,  $\alpha$  stiffness of the connector,  $I_p$  moment of inertia of the plaster cross-section, and  $E_{p,r}$  elastic modulus of the plaster, modified to take into account the second order effects. The  $E_{p,r}$  is evaluated according to the approach suggested in EC2 (§5.8.7.2) [52] and NTC 2018 (§4.1.2.3.9.3) [31] for the evaluation of buckling load in concrete columns as:

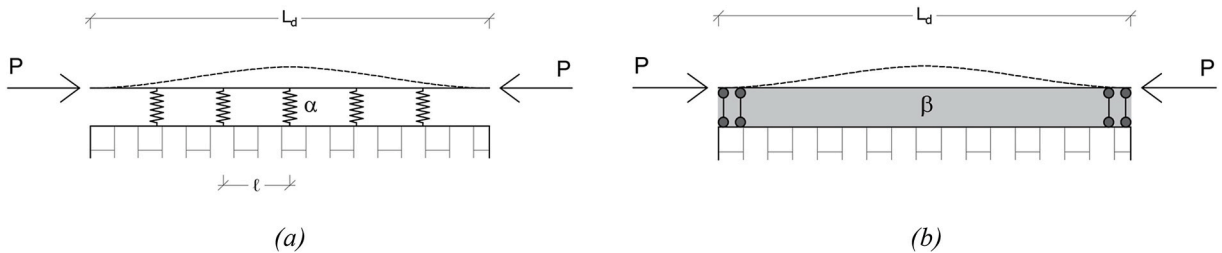


Fig. 4. (a) Model proposed by Papia et al. [53] with a discrete number of unilateral supports and (b) model proposed by Russo et al. [54] with an equivalent elastic medium.

$$E_{p,r} = \frac{0.3}{1 + 0.5\varphi} E_p \quad (12)$$

where  $\varphi$  is the viscosity coefficient assumed equal to 2 and  $E_p$  is the design elastic modulus of plaster.

Fig. 5 shows the critical load  $c_{cr}$  as a function of  $\gamma$  in a logarithmic scale.

The value of the critical load  $P_{cr}$  of the plaster strut can be found as:

$$P_{cr} = P_e \cdot c_{cr} \quad (13)$$

with the Euler's buckling load  $P_e$  evaluated as:

$$P_e = \frac{\pi^2 E_{p,r} I_p}{\ell^2} \quad (14)$$

For the evaluation of the anchor's stiffness  $\alpha$ , if experimental data are not available, an analytical formulation is proposed which considers both the axial and the bending deformability. Fig. 6a shows the anchors embedded in the wall, while Fig. 6b shows the associated free body diagram, where  $q$  are the bearing reaction forces acting on the length  $2L_q$  and  $h_{ef}$  is the embedment depth of the anchors in the masonry wall. Considering  $F = 1$ , the equilibrium for moments gives:

$$q = \frac{R - d/2}{L_q^2} \quad (15)$$

and the stiffness  $\alpha$  can be evaluate applying the virtual work equation as:

$$\alpha = \frac{1}{\frac{h_{ef} + \Delta L}{E_s A_s} + \frac{\pi(R-d/2)}{4E_s A_s} + \frac{q^2 L_q^5}{10E_s I_s} + \frac{(R-d/2)^2 L_q}{E_s I_s} - \frac{(R-d/2)q L_q^3}{3E_s I_s} + \frac{(R-d/2)^2 \Delta L}{E_s I_s} + \frac{\pi(R-d/2)^3}{4E_s I_s}} \quad (16)$$

where  $E_s$  is the steel elastic modulus,  $A_s$  is the cross-section area of the rebar,  $I_s$  is the second moment of area of the rebar section,  $d$  is the rebar diameter,  $R$  is the rebar outside bend radius and  $\Delta L$  is defined as in Fig. 6b.

The presence of initial imperfections (e.g., construction imperfections, eccentricity of the load) can further reduce the ultimate carrying capacity. The plaster maximum load  $N_{p,i}$ , which accounts also for initial imperfections, can be defined as:

$$N_{p,i} = i \cdot P_{cr} \quad (17)$$

where the reduction coefficient  $i$  is given by:

$$i = \left( 1 - \frac{U_\xi}{U_{max}} \right) \quad (18)$$

with  $U_\xi$  initial imperfection, expressed as an initial deflection of the strut, and  $U_{max}$  final maximum deflection of the strut. Further details on the evaluation of the imperfection effect can be found in Appendix A. The initial imperfection  $U_\xi$  can be evaluated according to Eurocode 2 (§4.3.5.4) [52] which says that “for individual structural elements (not frame), geometrical imperfections may be taken into account by increasing the eccentricity of the load with an additional eccentricity”. The additional eccentricity  $e_a$  is defined as:

$$e_a = U_\xi = \frac{\nu \ell}{2} \quad (19)$$

where  $\ell$  is the effective length of the structural element (i.e., spacing between anchors expressed in meters) and  $\nu$  is defined as:

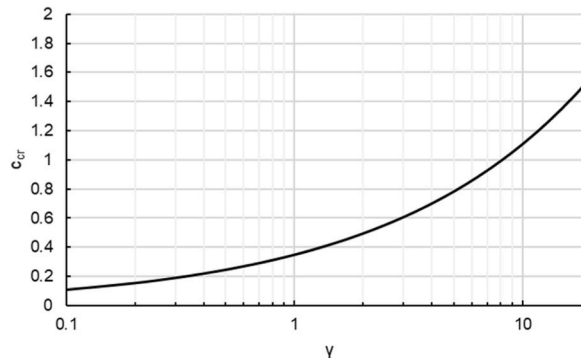


Fig. 5. Dimensionless critical load  $c_{cr}$  vs  $\gamma$ .

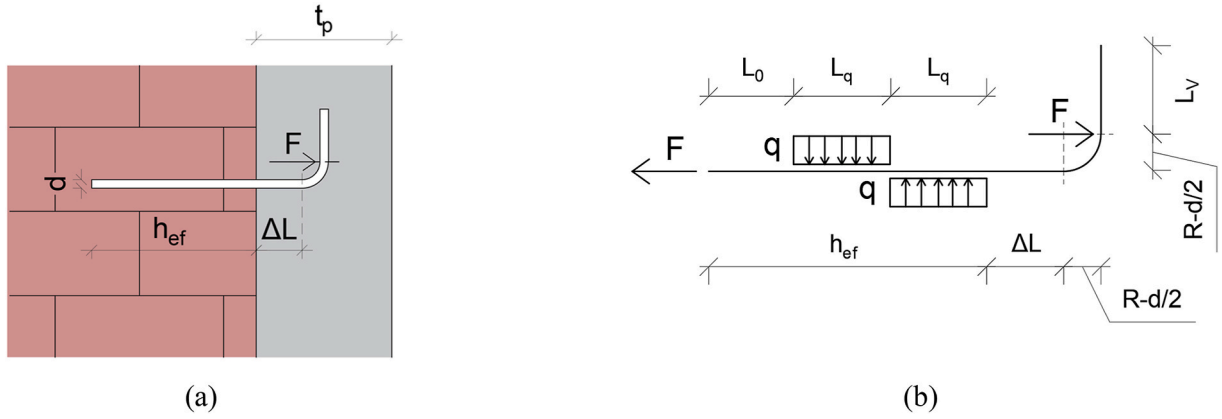


Fig. 6. (a) Anchor in the wall; (b) anchor free body diagram.

$$\nu = \frac{1}{100\sqrt{\epsilon}} \quad (\text{rad}) \quad (20)$$

A lower bound for  $\nu$  is set equal to  $\nu_{\min} = L/200$  according to Eurocode 2.

For the evaluation of the maximum deflection  $U_{\max}$ , a numerical parametric study was performed using the finite element software Abaqus [55]. The diagonal plaster strut was analyzed as a beam element subjected to axial compression, considering the presence of the initial imperfection and varying the number of connectors (i.e., their spacing) and the plaster thickness. For all the studied configurations, the values of maximum deflection at the 70% of the maximum load were collected and used to calibrate the following analytical expression:

$$U_{\max} = (\epsilon \cdot t_p + m)n \left( \delta \frac{t_p}{t_{\text{ref}}} - \omega \right) \quad (21)$$

where  $t_p$  is the plaster thickness,  $n$  is the number of anchors per square meter and  $\epsilon$ ,  $m$ ,  $\delta$ ,  $\omega$  and  $t_{\text{ref}}$  are constants, defined in order to fit the numerical results, with the following values:

$$\begin{aligned} \epsilon &= -0.0067 \\ m &= 16.377 \text{ mm} \\ \delta &= 0.13 \\ \omega &= 0.2773 \\ t_{\text{ref}} &= 100 \text{ mm} \end{aligned}$$

### 3. Assessment of the proposed approach

In this section, the assessment of the proposed model is presented using experimental results of diagonal compression tests conducted on masonry panel strengthened with SRP. The amount of data related to the tests presented by the authors [37] were limited, therefore results from other authors [38,39] were also used. It should be highlighted that, in general, the experimental data of diagonal compression tests related to SRP applied to masonry reported in the scientific literature are few. For this reason, it was not possible to perform first a calibration and then a testing of the proposed method, splitting the available results in two groups. Therefore, all the collected data [37–39] were used in the following assessment process.

#### 3.1. Experimental database

##### 3.1.1. Experimental researches

In the research presented by Biolzi et al. [37], a total of 10 clay brick walls, with two or three wythes thickness (i.e., 250 and 380 mm) were tested, 4 unreinforced and 6 strengthened by means of SRP with 30 or 50 mm thickness. For each layout, two specimens were tested. The experimental program was focused on the study of the influence of the geometry (i.e., wall and plaster thicknesses) on the bearing capacity of the specimens, while keeping constant all the other parameters. A cementitious mortar was used as plaster. The connectors [56] were 8 mm diameter steel ribbed bars bent to form a 90-degree hook at the outer end, in a number of 4.8 per square meter. A steel mesh of 6 mm diameter wire with a spacing of 100 mm in both horizontal and vertical directions was embedded in the plaster.

Gattesco et al. [57] tested a total of 60 masonry specimens strengthened with a mortar coating applied on both faces of the wall and reinforced with a glass fiber reinforced polymer (GFRP) mesh or a steel mesh. Four types of masonry, three different types of masonry mortar and five different GFRP meshes for the reinforcement were considered. For each configuration, two specimens were tested. From all the available data, the specimens considered for the validation were the one made of solid clay brick with two or three wythes



thickness (i.e. 250 and 380 mm) as in Ref. [37], with hydraulic lime mortar and steel mesh as reinforcement.

Additional test results were collected from the experimental program presented by Maddaloni [38] and performed on tuff masonry walls. A total of 34 retrofitted specimens were tested (plus 6 unreinforced), considering the application of the coating on one or two sides, with different type of reinforcement (GFRP or steel) and different typologies of coating mortar (fiber-reinforced lime mortar or cementitious mortar). The tests here analyzed include only the ones with steel as reinforcement, with the application of the mortar coating on both sides.

Table 1 resumes the main input data and the obtained experimental results for the analyzed configurations. A code has been assigned to identify the different tested layouts (B, G, and M identify the main author, URM and RM indicate the unreinforced and the retrofitted configurations, respectively),  $t_p$  and  $f_c$  are the thickness and the compressive strength of the mortar overlay,  $P_{max}$  is the maximum load obtained from the diagonal compression test (evaluated as the mean of the available test results), CoV is the coefficient of variation,  $\lambda_{ex}$  is the obtained increasing capacity coefficient.

### 3.1.2. Discussion on the experimental results

In all the campaigns, each test configuration has been tested twice (with the exception of M-URM-01); it is evident that the unreinforced specimens show higher scatter of the results (CoV from 13.3 to 46.0) with respect to the retrofitted ones (CoV from 0.5 to 14.7). This is due to the fact that the heterogeneity of the masonry material and the presence of weak areas in the unreinforced specimen can cause great variation of the resistance, also for twin specimens. On the other hand, the application of the plaster, made using a homogenous material, lends homogeneity to the retrofitted wall and a stabilizing effect in the fracture process. The lowest value of the amplification coefficient is 1.58 for the G-RM-03 configuration, which is higher than the maximum coefficient suggested by the Italian Standard for clay brick masonry which is 1.5 [31,32].

Some major differences between the compared configurations, that can affect the analytical results, should be highlighted. With respect to the experimental results of Biolzi et al., the considered tests from Gattesco et al. were performed on similar masonry specimens (solid clay brick), but with a quite lower compressive strength of the mortar overlay (6.71 vs 33.8 MPa). On the other side, the Maddaloni tests were performed on a different masonry typology (tuff). The plaster thickness, the number of anchors per square meter and the steel reinforcement vary, for the different configurations, in reasonable and limited ranges. It is also interesting to highlight that the experimental tests presented by Biolzi et al. showed an unexpected result in terms of the influence of the plaster thickness on the maximum load. Indeed, configurations B-RM-01 and B-RM-02 exhibited a similar load despite the different plaster thickness (30 and 50 mm). A possible explanation on this matter can be found in Ref. [37]. In any case, the result obtained for B-RM-02 configuration could be considered as an outlier.

Since the analyzed studies did not provide the compressive strength of the masonry walls, the assessment were performed considering the compressive strength evaluated from the properties of the masonry components (units + mortar). According to the results presented by Ferretti et al. [58], among the many available predictive models, the analytical formulation proposed by Dayaratnam [59] has been considered as the most suitable to evaluate the properties of “poor quality” masonry specimens. Table 2 reports the compressive strength of unit ( $f_b$ ) and mortar ( $f_j$ ), and the predicted masonry compressive strength ( $f_m$ ) for the different experimental programs.

### 3.2. Validation of the analytical results

Table 3 shows the results obtained using the proposed analytical method.  $P_{max}$  and  $\lambda_{ex}$  are the experimental maximum load and the

**Table 1**  
Experimental data for the validation of the method.

Reference	Code	Specimen		Mesh type [mm]	Plaster		Connectors [n°/mq]	N° of spec.	$P_{max}$ [kN]	CoV [–]	$\lambda_{ex}$ [–]
		Material	Size [mm]		$t_p$ [mm]	$f_c$ [MPa]					
Biolzi et al. [37]	B-URM-01	SCB + LM	1290x1290x250	–	–	–	–	2	198.7	23.9	–
	B-URM-02	SCB + LM	1290x1290x380	–	–	–	–	2	340.4	46.0	–
	B-RM-01	SCB + LM	1290x1290x250	$\phi 6$ @100	30	33.8	4.7	2	369.6	1.1	1.86
	B-RM-02	SCB + LM	1290x1290x250	$\phi 6$ @100	50	33.8	4.7	2	375.3	0.5	1.89
	B-RM-03	SCB + LM	1290x1290x380	$\phi 6$ @100	50	33.8	4.7	2	552.2	3.4	1.62
Gattesco et al. [57]	G-URM-01	SCB + LM	1160x1160x250	–	–	–	–	2	191.9	16.5	–
	G-URM-02	SCB + LM	1160x1160x380	–	–	–	–	2	285.7	13.3	–
	G-RM-01	SCB + LM	1160x1160x250	$\phi 5$ @150	30	6.7	6.0	2	332.0	3.1	1.73
	G-RM-02	SCB + LM	1160x1160x380	$\phi 5$ @150	30	6.7	6.0	2	451.1	14.7	1.58
Maddaloni [38]	M-URM-01	TM + LM	1200x1190x250	–	–	–	–	6	106.7	14.8	–
	M-RM-01	TM + LM	1200x1190x250	$\phi 6$ @100	40	14.5	3.5	2	322.0	14.5	3.02
	M-RM-02	TM + LM	1200x1190x250	$\phi 6$ @100	40	17.0	3.5	2	389.5	4.2	3.65
	M-RM-03	TM + LM	1200x1190x250	$\phi 6$ @100	40	18.8	3.5	2	417.5	10.6	3.91

Notes:LM: Lime Mortar, SCB: Solid Clay Brick, TM: Tuff Masonry



**Table 2**  
Compressive strength of unit, mortar and masonry.

Reference	$f_b$ MPa	$f_j$ MPa	$f_m$ MPa
Biolzi et al. [37]	23.30	5.40	3.08
Gattesco et al. [57]	44.00	2.60	2.95
Maddaloni [38]	5.40	6.40	1.62

respective amplification coefficient (as in Table 1),  $N_{max}$  and  $\lambda$  are the respective analytical values. Fig. 7 shows the comparison between the experimental and predicted values for unreinforced and retrofitted masonry walls, with the coefficient of determination  $R^2$  and the regression line. Fig. 8 presents the comparison in terms of the amplification coefficient  $\lambda$ .

The results for the unreinforced specimens (Fig. 7a) show an excellent agreement between the experimental and predicted values, with a coefficient of determination  $R^2$  equal to 0.9865 and a regression line almost coincident to the bisector. The safety factor, intended as the ratio between experimental and analytical prediction, resulted 1.03. It should be notice that this good agreement is strictly related to the fact that the experimental data of the unreinforced specimens were used to calibrate the width of the strut.

When considering both the unreinforced and the retrofitted results (Fig. 7b), the coefficient of determination  $R^2$  decreases to 0.673, with a safety factor equal to 1.20. Two points related to the retrofitted configurations are overestimated (Biolzi RP), and one of them is related to the configuration B-RM-02, whose experimental result was unexpected, as previously discussed. As a matter of fact, the influence of the plaster thickness on the bearing capacity was not evident from the results of tests B-RM-01 and B-RM-02, which showed similar load despite their different plaster thickness, resulting in an overestimation or underestimation of the analytical load for the two different configurations. However, the soundness of the analytical model is confirmed by the good fitting between the estimation and the experimental results obtained by the other considered authors. Indeed, a linear trend is clearly recognizable and the regression line still shows a slope similar to the bisector line, staying on the safe side of the plot. By removing the outlier result (i.e., B-RM-02) from the plot, the coefficient of determination  $R^2$  would increase to 0.7598.

With reference to the amplification coefficient  $\lambda$  (Fig. 8), a linear trend is still recognizable, even though the slope of the regression line has decreased (i.e., it is lower than the bisector slope), which indicates that the prediction should stay on the safe side. The safety factor is 1.17, while the coefficient of determination  $R^2$  is equal to 0.6592, which increases to 0.8314 if the outlier result (i.e., B-RM-02) is not considered.

The empirical formulation proposed by the NTC 2018 for the evaluation of the performance of SRP retrofitted walls suggests a maximum amplification coefficient equal to 1.5 for the brickwork masonry and 1.7 for the tuff masonry, regardless of the actual design parameters. These coefficients result, in most of the cases, conservative with respect to both the obtained analytical and experimental results, especially for the tuff masonry.

#### 4. Parametric study

A parametric study was performed in order to examine the sensitivity of the proposed model to a set of parameters including the masonry and coating mortar compressive strength and thickness and the number of anchors per square meter. The influence of the main parameters related to the masonry (i.e., masonry compressive strength and thickness) have a proportional linear effect on the maximum load, so the respective plots are omitted. It must be highlighted that, due to the poor quantity of available experimental data, the obtained results could not be properly verified. Nevertheless, it seems interesting to show them to well understand how the model works and make some general considerations. The parameters range has been chosen according to the most common values adopted in the job sites. For the not explicit parameters, the following values have been considered:  $f_m = 3.45$  MPa,  $t_m = 250$  mm,  $f_c = 20$  MPa,  $t_p = 30$  mm,  $n = 5$ . The steel mesh and the connectors has been defined according to the ones adopted in Ref. [37].

**Table 3**  
Experimental and analytical results.

Specimen	$P_{max}$ kN	$\lambda_{ex}$ –	$N_{max}$ kN	$\lambda$ –
B-URM-01	198.7	–	211.0	–
B-URM-02	340.4	–	320.8	–
B-RM-01	369.6	1.86	356.0	1.69
B-RM-02	375.3	1.89	508.0	2.41
B-RM-03	552.5	1.62	617.8	1.93
G-URM-01	191.9	–	181.3	–
G-URM-02	285.7	–	275.6	–
G-RM-01	332.0	1.73	241.3	1.33
G-RM-02	451.1	1.58	335.6	1.22
M-URM-01	106.7	–	102.9	–
M-RM-01	322.0	3.02	264.0	2.57
M-RM-02	389.5	3.65	270.6	2.63
M-RM-03	417.5	3.91	274.8	2.67

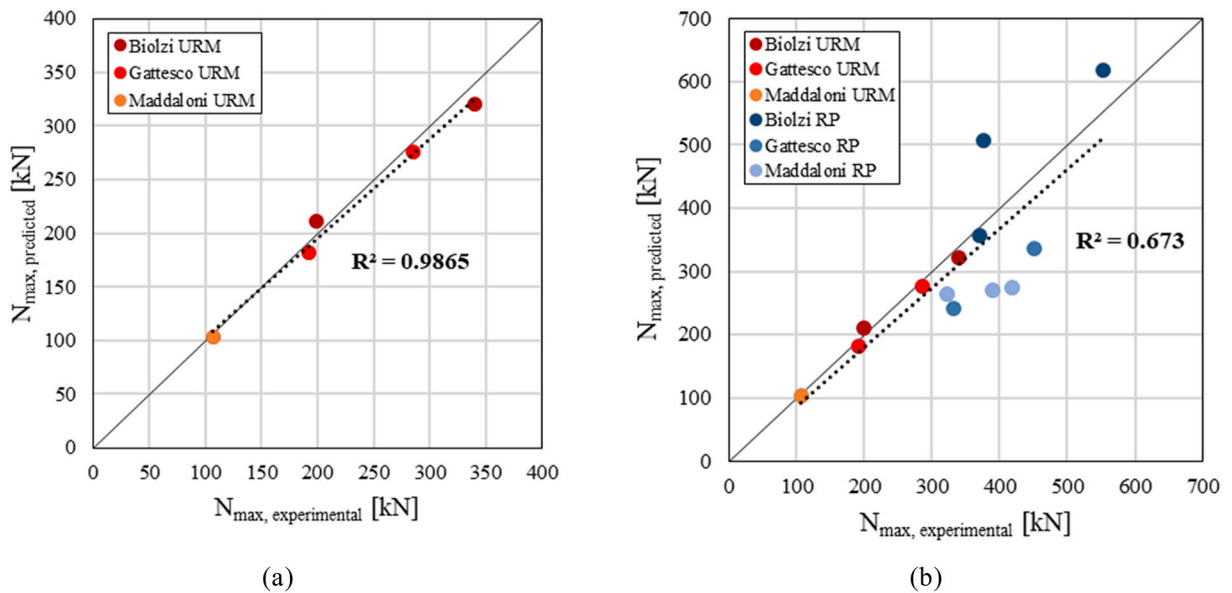


Fig. 7. Experimental and predicted load for (a) unreinforced and (b) unreinforced + retrofitted masonry. URM refers to unreinforced specimens while RP to retrofitted ones.

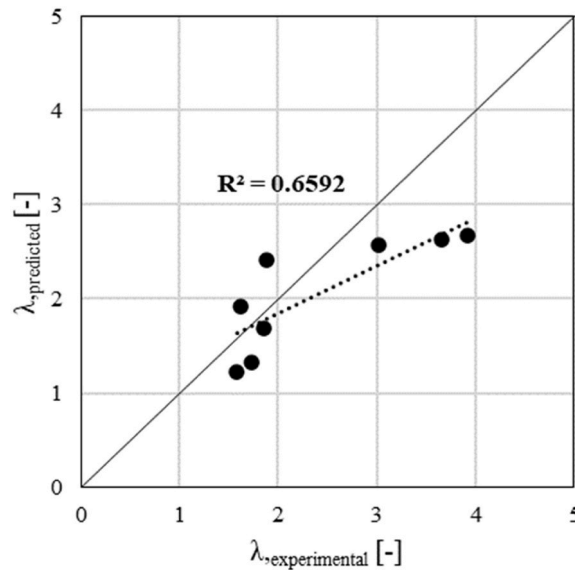


Fig. 8. Experimental and predicted value of the amplification coefficient  $\lambda$ .

#### 4.1. Number of anchors

Fig. 9 shows the influence of the number of anchors on the maximum load. It is evident that the number of anchors affect the final load but, in most of the studied cases, above a certain value, the load increase becomes limited or vanishes. For low value of compressive strength of the plaster ( $f_c = 10$  MPa in Fig. 9a), the effect of the anchor increase becomes neglectable above 7 anchors, which correspond to the activation of the crushing failure mechanism. Higher compressive strength prevents instead the failure for crushing, making the slope variation less significant but still evident. When considering a low thickness of the plaster ( $t_p = 15$  in Fig. 9b), the predominant mechanism remains always the instability failure, with the load increasing proportionally to the increase of the number of anchors (constant slope). For higher plaster thickness, the buckling mechanism can be prevented using an adequate number of anchors. But again, beyond a certain value (e.g., 8 anchors for  $t_p = 30$  mm), a further increase of the number of anchors does not have any additional positive effect on the load. It can be stated that the optimal number of anchors is strictly related to the properties of the plaster cover and to its crushing failure limit load. However, for the most common values of plaster compressive strength and thickness, the optimal number of anchors may range between 5 and 8 per square meter.

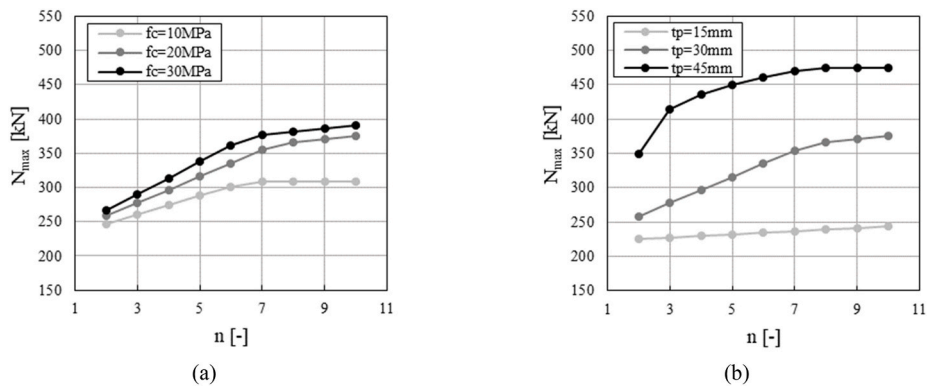


Fig. 9. Effect of the number of anchors per square meter on the maximum load (a) for different compressive strength of the plaster and (b) for different plaster thickness.

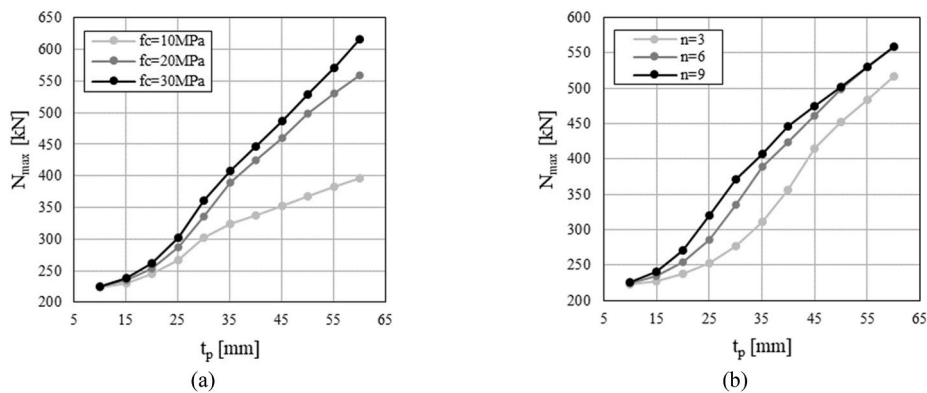


Fig. 10. Effect of the plaster thickness on the maximum load (a) for different compressive strength of the plaster and (b) for different number of anchors.

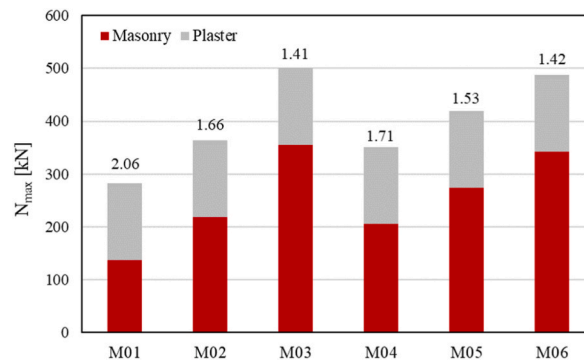


Fig. 11. Masonry and plaster contributions for different masonry properties.

It should be also highlighted that the position of the anchors in the wall may influence the load carrying capacity, depending on the direction of the applied load. For instance, a concentration of anchors along the compressed diagonal, which is usually the most damaged area of the specimen where the detachment from the masonry substrate happens first [37], may result in a higher capacity. However, in real applications, the quincunx configuration is usually adopted, which means having an approximately constant number of anchors per square meter, which is also the hypothesis made in the analytical model.

#### 4.2. Plaster thickness and compressive strength

Fig. 10 shows the effect of the plaster thickness on the maximum load with the change of the plaster compressive strength (a) and the number of anchors per square meter (b). In all the configurations, it is evident that a first branch of the curve describes an exponential trend, which is followed by a linear increase of the load that is associated to a crushing failure mechanism. For the same

number of anchors (Fig. 10a), the load increases faster for lower thicknesses, so the connectors result more effective if the plaster thickness is limited. Keeping constant the plaster compressive strength (Fig. 10b), the end of the exponential branch is shifted to higher thicknesses if the number of connectors decreases. Moreover, considering higher numbers of anchors for higher plaster thickness, the crushing failure becomes predominant and the load does not further increase with the number of anchors anymore.

The most common plaster thickness usually range between 30 and 60 mm. However, the effect of the thickness on the performance also depends on the masonry geometrical and mechanical properties. Fig. 11 shows the masonry and plaster load contributions for six different design configurations, together with the amplification coefficients. The reinforcement parameters are constant (in particular,  $t_p = 30$  cm,  $f_c = 30$  MPa), while the masonry thickness changes in M01 ( $t_m = 250$  mm,  $f_m = 2$  MPa), M02 ( $t_m = 400$  mm,  $f_m = 2$  MPa) and M03 ( $t_m = 650$  mm,  $f_m = 2$  MPa) and the compressive strength changes in M04 ( $f_m = 3$  MPa,  $t_m = 250$  mm), M05 ( $f_m = 4$  MPa,  $t_m = 250$  mm) and M06 ( $f_m = 5$  MPa,  $t_m = 250$  mm). It is clearly evident that for lower masonry thickness and mechanical properties, the beneficial effect of the retrofitting are more emphasized (i.e., higher values  $\lambda$ ).

## 5. Relevance of the research

SRP is one of the most employed conventional methods to strengthen common masonry constructions thanks to its simple technology, the use of ordinary and cheap materials and its effectiveness. Several technical codes recommend it as an effective retrofitting solution, without providing proper formulation to be used for the design. The proposed analytical approach could become a useful tool for practitioners, to achieve an accurate evaluation of the mechanical properties of masonry retrofitted with SRP, taking into account all the main design parameters (i.e., mechanical properties and thickness of masonry and plaster cover, as well as mechanical properties, geometry, and number of connectors). The method could replace the empirically-based formulations usually adopted for the design, which neglect the actual configuration of the reinforcement, leading to unconservative or uneconomical design solutions.

## 6. Conclusions

Although many innovative retrofitting methods have been proposed in the recent past, SRP remains one of the most common conventional techniques adopted to strengthen unreinforced masonry buildings thanks to its low cost and high performance. However, no specific guidelines are available nor valid theoretical models to design SRP interventions, with the consequence of often obtaining unsafe or uneconomical solutions. The present work proposed an analytical approach to predict the mechanical properties of walls retrofitted with SRP. The method was defined starting from diagonal tests results previously presented by the authors, considering also additional experimental data available in literature. The following main conclusions can be drawn:

- The proposed method evaluates the mechanical properties of masonry strengthened with SRP on the basis of the predictions of the load carrying capacity of unreinforced and retrofitted specimens subjected to diagonal compression tests.
- The calculation of the retrofitted wall resistance is conducted by adding to the URM resistance that of the coating layers, considering for them two alternative failure modes: crushing or buckling.
- The predicted carrying capacity for the unreinforced masonry wall is able to match the experimental loads with an excellent approximation ( $R^2 = 0.9865$ ).
- When considering also the retrofitted specimens, the accuracy prediction decreases ( $R^2 = 0.673$ ), even though the analytical results are conservative against the experimental values in most of the cases, with a very good trend proved by the regression line which almost overlaps the bisector line. Similar results are obtained for the amplification coefficient  $\lambda$ , evaluated as the ration between the carrying capacity of the retrofitted and unreinforced masonry.
- As qualitative indications for the design, a proper number of connectors must be considered to avoid the detachment of the plaster layers and the activation of instability phenomena, even though a further increase of this number after a certain value does not have any additional positive effect.

The presented results showed that the proposed method can be a useful tool to support the design of SRP retrofitting interventions, accounting for the main design parameters, with an acceptable level of accuracy, and a trend which locates the predicted results on the safe side.

It should be remarked that the quantity of available experimental data adopted to assess the method are too few and limited to clay brick and tuff masonry making unreliable any statistical treatment of the them. Further experimental results are required to give general validity to the proposed formulation and confirm the good trend of the prediction model. For this reason, additional experimental tests have been planned by the authors to investigate a wider range of design parameters (e.g., connectors, plaster mechanical properties) and increase the amount of experimental data essential for a satisfactory validation process.

## Author statement

Manuela Scamardo: Conceptualization, Methodology, Validation, Formal analysis, Investigation, Data curation, Writing - Original Draft, Writing - Review & Editing, Visualization. Sara Cattaneo: Conceptualization, Methodology, Investigation, Writing - Review & Editing, Supervision, Project administration. Pietro Crespi: Conceptualization, Methodology, Investigation, Writing - Review & Editing. Luigi Biolzi: Conceptualization, Methodology, Writing - Review & Editing, Supervision.

## Declaration of competing interest

The authors declare that they have no known competing financial interests or personal relationships that could have appeared to influence the work reported in this paper.

## Data availability

The authors do not have permission to share data.

## Appendix A

Initial geometrical and constitutive imperfections may produce a significant decrease of the capacity of a structural element. Considering a beam element with length  $L$  subjected to axial compression (Figure A1), the imperfection can be represented as an initial deflection shape  $\bar{v}(x)$  of the element, which can be expressed by the following sinusoidal function:

$$\bar{v}(x) = U_{\xi} \sin \frac{\pi x}{L} \quad (\text{A.1})$$

where  $U_{\xi}$  is the maximum initial deflection at the midpoint.

The element deflection produced by the axial load  $P$  is influenced by the initial deflection. The final shape of the element can be evaluated as:

$$v(x) = U_{\xi} \frac{1}{1 - P/P_e} \sin \frac{\pi x}{L} \quad (\text{A.2})$$

where  $P_e$  is the Euler's critical load.

The final maximum deflection at midpoint  $U_{\max}$  can be evaluated as:

$$v\left(\frac{L}{2}\right) = U_{\max} = U_{\xi} \frac{1}{1 - P/P_{cr}} \quad (\text{A.3})$$

From equation (A.3), it is possible to find that:

$$P = P_e \left( 1 - \frac{U_{\xi}}{U_{\max}} \right) \quad (\text{A.4})$$

which can be used to determine the value of the maximum load  $P$  when the beam is affected by imperfections (i.e., initial deflection).

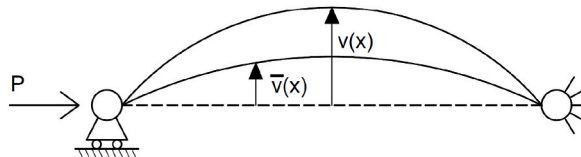


Fig. A.1. Beam element subjected to compression with initial deflection.

## References

- [1] S. Lagomarsino, Damage assessment of churches after L'aquila earthquake (2009), *Bull. Earthq. Eng.* 10 (2012) 73–92, <https://doi.org/10.1007/s10518-011-9307-x>.
- [2] G. Fiorentino, A. Forte, E. Pagano, F. Sabetta, C. Baggio, D. Lavorato, C. Nuti, S. Santini, Damage patterns in the town of amatrice after august 24th 2016 Central Italy earthquakes, *Bull. Earthq. Eng.* 16 (2018) 1399–1423, <https://doi.org/10.1007/s10518-017-0254-z>.
- [3] A. Penna, P. Morandi, M. Rota, C.F. Manzini, F. da Porto, G. Magenes, Performance of masonry buildings during the emilia 2012 earthquake, *Bull. Earthq. Eng.* 12 (2014) 2255–2273, <https://doi.org/10.1007/s10518-013-9496-6>.
- [4] R.K. Adhikari, D. D'Ayala, Nepal earthquake: seismic performance and post-earthquake reconstruction of stone in mud mortar masonry buildings, *Bull. Earthq. Eng.* 2020 (2015) 18, <https://doi.org/10.1007/s10518-020-00834-y>.
- [5] E.A. Godínez-Domínguez, A. Tena-Colunga, L.E. Pérez-Rocha, H.I. Archundia-Aranda, A. Gómez-Bernal, R.P. Ruiz-Torres, J.L. Escamilla-Cruz, The september 7, 2017 tehuantepec, Mexico, earthquake: damage assessment in masonry structures for housing, *Int. J. Disaster Risk Reduc.* (2021) 56, <https://doi.org/10.1016/j.ijdrr.2021.102123>.
- [6] G. Vlachakis, E. Vlachaki, P.B. Lourenço, Learning from failure: damage and failure of masonry structures, after the 2017 lesvos earthquake (Greece), *Eng. Fail. Anal.* (2020) 117.
- [7] M. Scamardo, A. Franchi, P. Crespi, An innovative approach for the finite element modelling of masonry cracking, in: *Proceedings of the Proceedings of the 10th International Masonry Conference, The International Masonry Society, Milano, 2018*, pp. 132–144, 0.
- [8] A. Giordano, E. Mele, A. de Luca, Modelling of historical masonry structures: comparison of different approaches through a case study, *Eng. Struct.* 24 (2002) 1057–1069, [https://doi.org/10.1016/S0141-0296\(02\)00033-0](https://doi.org/10.1016/S0141-0296(02)00033-0).
- [9] G. Magenes, A. della Fontana, Simplified non-linear seismic analysis of masonry buildings, in: *Proceedings of the Proceedings of the Fifth International Masonry Conference, 1998*, pp. 190–195.

- [10] M. Scamardo, A. Franchi, P.G. Crespi, A constitutive model for rubble masonry allowing for spread micro-cracks and localized macro-cracks, in: P. Roca, L. Pelà, C. Molins (Eds.), *Proceedings of the 12th International Conference on Structural Analysis of Historical Constructions SAHC 2020*, 2020, pp. 1699–1700.
- [11] S. Bhattacharya, S. Nayak, S.C. Dutta, A critical review of retrofitting methods for unreinforced masonry structures, *Int. J. Disaster Risk Reduc.* 7 (2014) 51–67, <https://doi.org/10.1016/j.ijdrr.2013.12.004>.
- [12] F. Yavartanoo, T.H.K. Kang, Retrofitting of unreinforced masonry structures and considerations for heritage-sensitive constructions, *J. Build. Eng.* 49 (2022), 103993, <https://doi.org/10.1016/j.jobe.2022.103993>.
- [13] N. Longarini, P. Crespi, A. Franchi, N. Giordano, P. Ronca, M. Scamardo, Cross-lam roof diaphragm for the seismic retrofitting of historical masonry churches, in: *Proceedings of the Proceedings of the International Masonry Society Conferences*, 2018, 0.
- [14] M. Scamardo, P. Crespi, N. Longarini, M. Zucca, Seismic vulnerability and retrofitting of a historical masonry building, in: *Proceedings of the Congress on Construction Pathology, Rehabilitation Technology and Heritage Management - REHABEND 2022*, Granada, 2022, pp. 787–794.
- [15] M. Miani, C. di Marco, G. Frappa, M. Pauletta, Effects of dissipative systems on the seismic behavior of irregular buildings—two case studies, *Buildings* 10 (2020), <https://doi.org/10.3390/buildings10110202>.
- [16] Y.-H. Jin, Z.-Y. Zhou, B.-L. Bao, H.-Y. Wang, T. Wang, Experimental study on the seismic performance of clay brick masonry wall strengthened with stainless steel strips, *J. Build. Eng.* 69 (2023), 106076, <https://doi.org/10.1016/j.jobe.2023.106076>.
- [17] M. ElGawady, P. Lestuzzi, M. Badoux, Retrofitting of masonry walls using shotcrete, *NZSEE Conf.* (2006) 45–54, 2006.
- [18] J.A.P.P. Almeida, E.B. Pereira, J.A.O. Barros, Assessment of overlay masonry strengthening system under in-plane monotonic and cyclic loading using the diagonal tensile test, *Construct. Build. Mater.* 94 (2015) 851–865, <https://doi.org/10.1016/j.conbuildmat.2015.07.040>.
- [19] S.S. Lucchini, L. Facconi, F. Minelli, G. Plizzari, Retrofitting unreinforced masonry by steel fiber reinforced mortar coating: uniaxial and diagonal compression tests, *Mater. Struct./Mater. Construct.* 53 (2020) 1–22, <https://doi.org/10.1617/s11527-020-01574-w>.
- [20] M. del Zoppo, M. di Ludovico, A. Balsamo, A. Prota, In-plane shear capacity of tuff masonry walls with traditional and innovative composite reinforced mortars (CRM), *Construct. Build. Mater.* (2019) 210, <https://doi.org/10.1016/j.conbuildmat.2019.03.133>.
- [21] S. Cattaneo, N. Vafa, Tensile capacity of adhesive anchors in damaged masonry, *Appl. Sci.* 11 (2021), <https://doi.org/10.3390/app11210135>.
- [22] M.R. Valluzzi, D. Tinazzi, C. Modena, Shear behavior of masonry panels strengthened by FRP laminates, *Construct. Build. Mater.* 16 (2002) 409–416, [https://doi.org/10.1016/S0950-0618\(02\)00043-0](https://doi.org/10.1016/S0950-0618(02)00043-0).
- [23] F. Ceroni, A. Garofano, M. Pecce, *Finite Element Modelling of Masonry Panels Reinforced with FRP Grids*, 2010.
- [24] H. Kolsch, Carbon fiber cement matrix (CFCM) overlay system for masonry strengthening, *J. Compos. Construct.* 2 (1998) 105–109, [https://doi.org/10.1061/\(ASCE\)1090-0268.1998.2:2\(105\)](https://doi.org/10.1061/(ASCE)1090-0268.1998.2:2(105)).
- [25] P. Meriggi, S. de Santis, S. Fares, G. de Felice, Design of the shear strengthening of masonry walls with fabric reinforced cementitious matrix, *Construct. Build. Mater.* (2021) 279, <https://doi.org/10.1016/j.conbuildmat.2021.122452>.
- [26] T. D'Antino, F.G. Carozzi, C. Poggi, Diagonal shear behavior of historic walls strengthened with composite reinforced mortar (CRM), *Mater. Struct./Mater. Construct.* 52 (2019) 1–15, <https://doi.org/10.1617/s11527-019-1414-1>.
- [27] E. Esmaeili, E. Manning, J.A.O. Barros, Strain hardening fibre reinforced cement composites for the flexural strengthening of masonry elements of ancient structures, *Construct. Build. Mater.* 38 (2013) 1010–1021, <https://doi.org/10.1016/j.conbuildmat.2012.09.065>.
- [28] M.A. Najafgholipour, S.M. Dehghan, A.R. Kamrava, In-plane shear behavior of masonry walls strengthened with steel fiber-reinforced concrete overlay, *Asian J. Civil Eng.* 19 (2018), <https://doi.org/10.1007/s42107-018-0041-4>.
- [29] M.A. Elgawady, P. Lestuzzi, A review of conventional seismic retrofitting techniques for URM, 13th Int.l Brick Block Masonry Conf. 1–10 (2004).
- [30] Ministero dei Lavori Pubblici Decreto Ministero Dei Lavori Pubblici 2 Luglio, 1981 - normativa per le riparazioni ed il rafforzamento degli edifici danneggiati dal sisma nelle regioni basilicata, Campania e Puglia (1981).
- [31] Ministero delle Infrastrutture e dei Trasporti Decreto Ministeriale 17 Gennaio, in: C.S.LL.PP. Aggiornamento Delle «Norme Tecniche Per Le Costruzioni» 2018, 2018.
- [32] Ministero delle Infrastrutture e dei Trasporti Circolare 21 gennaio 2019, n. 7 C.S.LL.PP. Istruzioni per l'applicazione Dell'«Aggiornamento delle norme tecniche per, Le Costruzioni» 1–14 (2019).
- [33] Earthquake planning and protection organization of Greece eppo code of interventions, KAN.EPE.) 1–337 (2013).
- [34] Federal Emergency Management Agency, American Society of Civil Engineers *FEMA 356 Prestandard and Commentary for the Seismic Rehabilitation of Buildings*, 2000.
- [35] S. Churilov, E. Dumova-Jovanoska, In-plane shear behaviour of unreinforced and jacketed brick masonry walls, *Soil Dynam. Earthq. Eng.* 50 (2013) 85–105, <https://doi.org/10.1016/j.soildyn.2013.03.006>.
- [36] B. Ghiassi, M. Soltani, A.A. Tasnimi, Seismic Evaluation of Masonry Structures Strengthened with Reinforced Concrete Layers, 2012, 10.1061/(ASCE)ST.1943-541X.
- [37] L. Biolzi, S. Cattaneo, P. Crespi, M. Scamardo, N. Vafa, Diagonal compression cyclic testing of unreinforced and reinforced masonry walls, *Construct. Build. Mater.* (2023) 363.
- [38] G. Maddaloni, *Analisi Sperimentale Del Comportamento Di Edifici in Muratura Rinforzati Con Tecniche e Materiali Innovativi*, 2017.
- [39] N. Gattesco, I. Boem, Experimental and analytical study to evaluate the effectiveness of an in-plane reinforcement for masonry walls using GFRP meshes, *Construct. Build. Mater.* 88 (2015) 94–104, <https://doi.org/10.1016/j.conbuildmat.2015.04.014>.
- [40] L. Facconi, S.S. Lucchini, F. Minelli, G.A. Plizzari, Analytical model for the in-plane resistance of masonry walls retrofitted with steel fiber reinforced mortar coating, *Eng. Struct.* 275 (2023), 115232, <https://doi.org/10.1016/j.engstruct.2022.115232>.
- [41] P. Crespi, S. Cattaneo, M. Scamardo, N. Vafa, Steel mesh reinforced coating characterization for masonry upgrading, in: *Proceedings of the Congress on Construction Pathology, Rehabilitation Technology and Heritage Management - REHABEND 2022*, Granada, 2022, pp. 1980–1988.
- [42] J. Segura, L. Pelà, S. Saloustros, P. Roca, Experimental and numerical insights on the diagonal compression test for the shear characterisation of masonry, *Construct. Build. Mater.* 287 (2021), 122964, <https://doi.org/10.1016/j.conbuildmat.2021.122964>.
- [43] A. Brignola, S. Frumento, S. Lagomarsino, S. Podestà, Identification of shear parameters of masonry panels through the in-situ diagonal compression test, *Int. J. Architect. Herit.* 3 (2009) 52–73, <https://doi.org/10.1080/15583050802138634>.
- [44] C. Calderini, S. Cattari, S. Lagomarsino, The use of the diagonal compression test to identify the shear mechanical parameters of masonry, *Construct. Build. Mater.* 24 (2010) 677–685, <https://doi.org/10.1016/j.conbuildmat.2009.11.001>.
- [45] B.S. Smith, Lateral stiffness of infilled frames, *J. Struct. Div.* 88 (1962), <https://doi.org/10.1061/jsdeag.0000849>.
- [46] A. Madan, A.M. Reinhorn, J.B. Mander, R.E. Valles, Modeling of masonry infill panels for structural analysis, *J. Struct. Eng.* 123 (1997), 10.1061/(asce)0733-9445(1997)123:10(1295).
- [47] B. Stafford Smith, Behavior of square infilled frames, *J. Struct. Div.* (1966) 92.
- [48] A. Saneinejad, B. Hobbs, Inelastic design of infilled frames, *J. Struct. Eng.* 121 (1995), [https://doi.org/10.1061/\(asce\)0733-9445.1995.121:4\(634](https://doi.org/10.1061/(asce)0733-9445.1995.121:4(634).
- [49] FEMA 356 FEMA 356 Prestandard, in: *US Federal Emergency Management Agency*, 2000, 2000.
- [50] N. Tarque, L. Candido, G. Camata, E. Spacone, Masonry infilled frame structures: state-of-the-art review of numerical modelling, *Earthquake Struct.* 8 (2015) 225–251, <https://doi.org/10.12989/eas.2015.8.1.225>.
- [51] M. Scamardo, S. Cattaneo, L. Biolzi, N. Vafa, Parametric analyses of the response of masonry walls with reinforced plaster, *Appl. Sci.* 12 (2022), <https://doi.org/10.3390/app12105090>.
- [52] European Committee for Standardization, EN 1992-1-1, Eurocode 2: design of concrete structures - Part 1-1, Gen. Rules Rules Buildi. Eurocode (2004).
- [53] M. Papia, G. Russo, G. Zingone, Instability of longitudinal bars in RC columns, *J. Struct. Eng.* 114 (1988) 445–461.
- [54] G. Russo, L. Terenzani, Non linear buckling model of the longitudinal reinforcement of RC columns, *Stud. Res.* 22 (2001) 203–227.
- [55] Dassault Systèmes, ABAQUS/CAE Documentation, 2017.
- [56] ETA-22/0395 hilti injection system HIT-HY 270 in solid bricks, *Metal Inject. Anchors Use Masonry* (2022).

- [57] N. Gattesco, I. Boem, A. Dudine, Diagonal compression tests on masonry walls strengthened with a GFRP mesh reinforced mortar coating, *Bull. Earthq. Eng.* 13 (2015) 1703–1726, <https://doi.org/10.1007/s10518-014-9684-z>.
- [58] F. Ferretti, C. Mazzotti, Brick masonry compressive strength evaluation: comparison between predictive models, in: *Proceedings of the REHABEND 2020 Construction Pathology, Rehabilitation Technology and Heritage Management*, Granada, 2020.
- [59] Dayaratnam, P *Brick and Reinforced Brick Structures*, Oxford & IBH, 1987.